Electronic Supplementary Material (ESI) for Materials Horizons.

Supplementary Information for

Hierarchically distributed microstructure design of haptic sensors for personalized fingertip mechanosensational manipulation

Xinqin Liao[a], Wensong Wang[a], Maohua Lin[b], Minghua Li[c], Hualin Wu[c] & Yuanjin Zheng[a]

[a] School of Electrical and Electronic Engineering, Nanyang Technological University, 50 Nanyang Avenue, Singapore 639798, Singapore

[b] Department of Ocean & Mechanical Engineering, Florida Atlantic University, 777 Glades Road, Boca Raton, 33431, USA

[c] School of Materials Science and Engineering, University of Science and Technology Beijing, 30 Xueyuan Road, Haidian District, Beijing 100083, China

Correspondence and requests for materials are addressed to X.L. (liaoxinqin677@163.com) or Y.Z. (yjzheng@ntu.edu.sg).

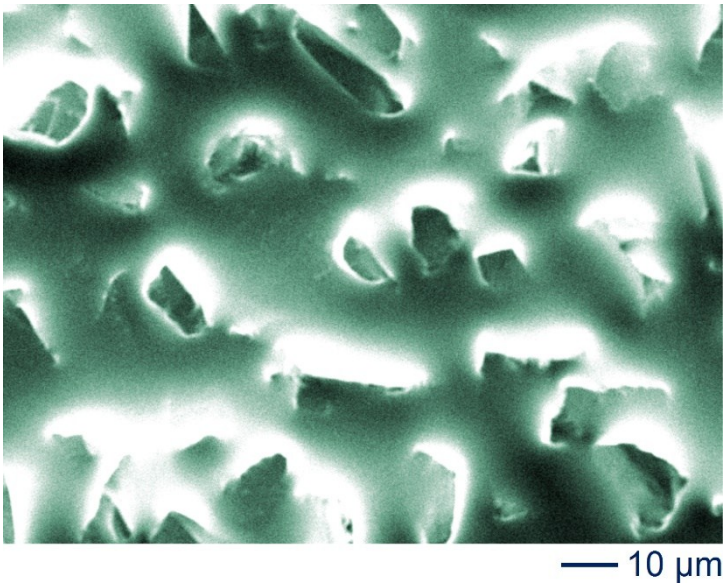

Fig. S1. FESEM image of pure abrasive paper (200 mesh).

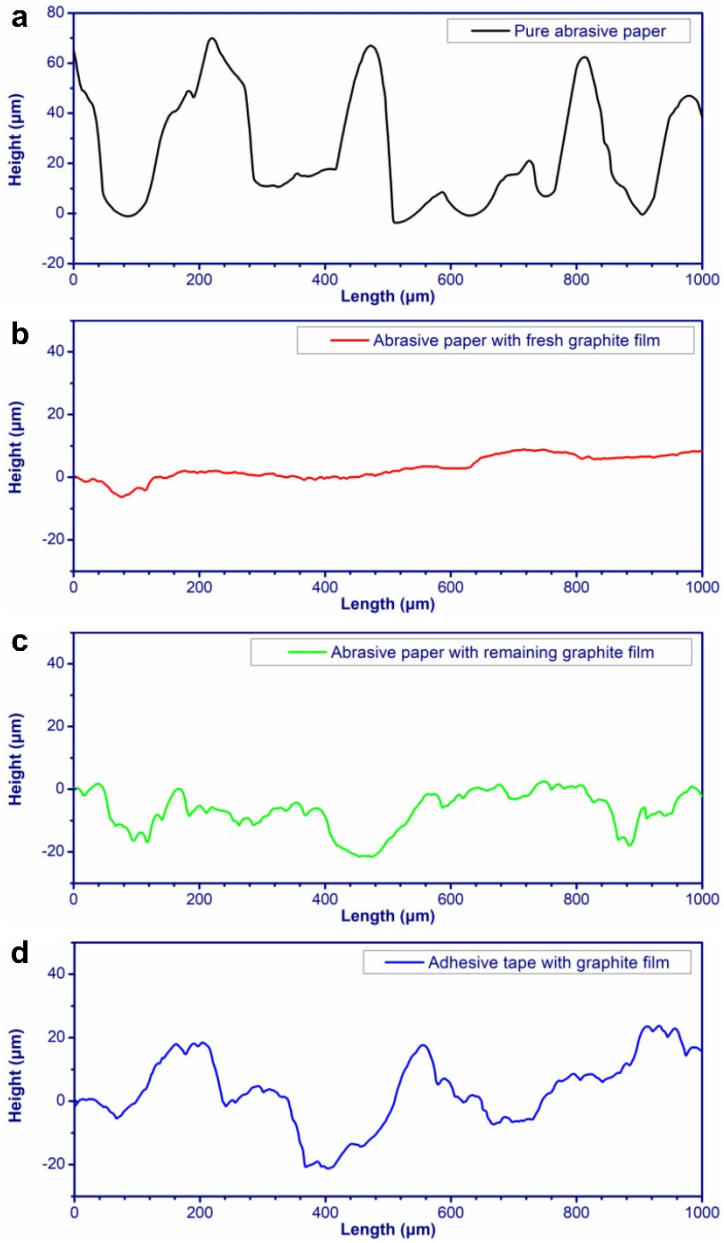

Fig. S2. Roughness profiles of (**a**) pure abrasive paper, (**b**) abrasive paper with fresh graphite film, (**c**) abrasive paper with remaining graphite film, and (**d**) adhesive tape with graphite film.

Here, the roughness (R_a) of the pure abrasive paper was 18.5 μm. The roughness of the abrasive paper with fresh graphite film, the abrasive paper with remaining graphite film, and the adhesive tape with graphite film were 1.56 μm, 5.03 μm, and 5.42 μm, respectively.

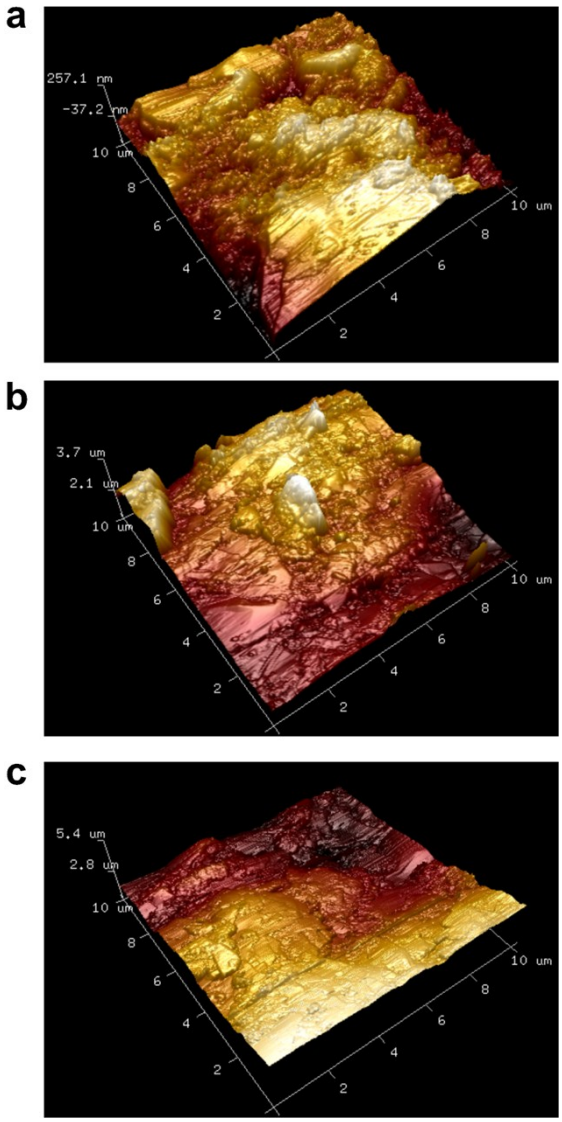

Fig. S3. Typical atomic force microscope (AFM) topography images of (a) abrasive paper with fresh graphite film, (b) abrasive paper with remaining graphite film, and (c) adhesive tape with graphite film.

Here, the roughness (R_a') of the abrasive paper with fresh graphite film, the abrasive paper with remaining graphite film, and the adhesive tape with graphite film were 62 ± 15 nm, 262 ± 83 nm, and 274 ± 85 nm, respectively, by measuring 10 samples. The values of the Ra' from AFM were lower than that of roughness profiles from Dektak XT surface profiler, which was due to the fact that the relatively small area could be scanned by AFM. Even so, the results together indicated that the surfaces of the abrasive paper with remaining graphite film and the adhesive tape with graphite film were rougher than the one of the abrasive paper with fresh graphite film.

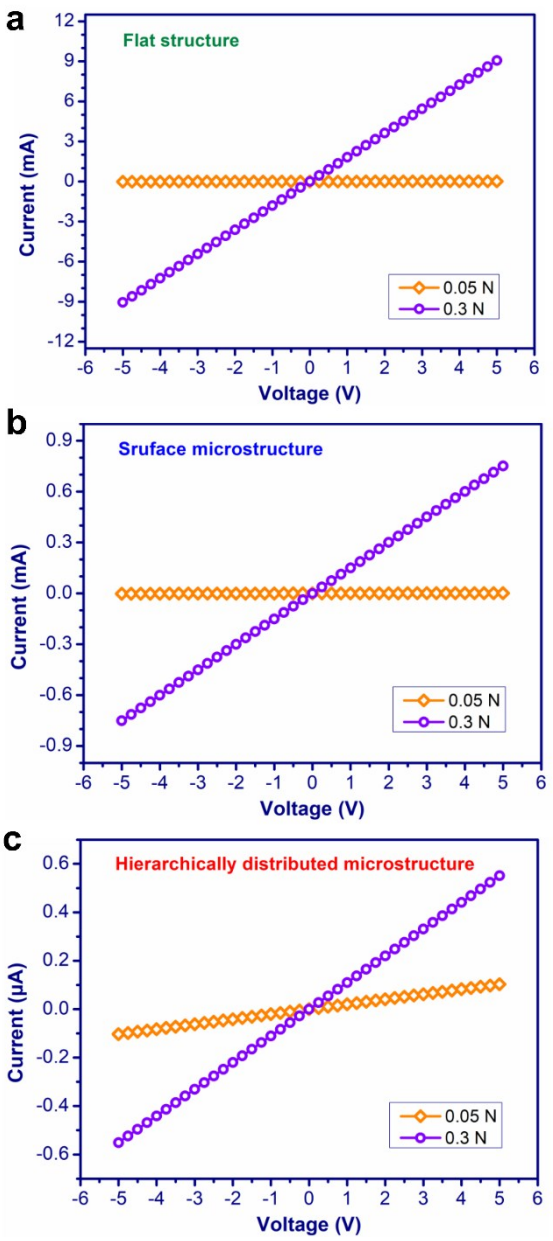

Fig. S4. Current-voltage (*I-V*) characteristic curves of the (**a**) FS haptic sensor, (**b**) SM haptic sensor, and (**c**) HDM haptic sensor under the external force of 0.05 and 0.3 N. It can be found that the current of the three types of haptic sensors is changed at the same voltage when the external force is applied. Nevertheless, no matter they are subjected to external force or not, all the curves are linear, implying ohmic characteristic. Thus, the as-prepared haptic sensors all belong to resistance-type devices.

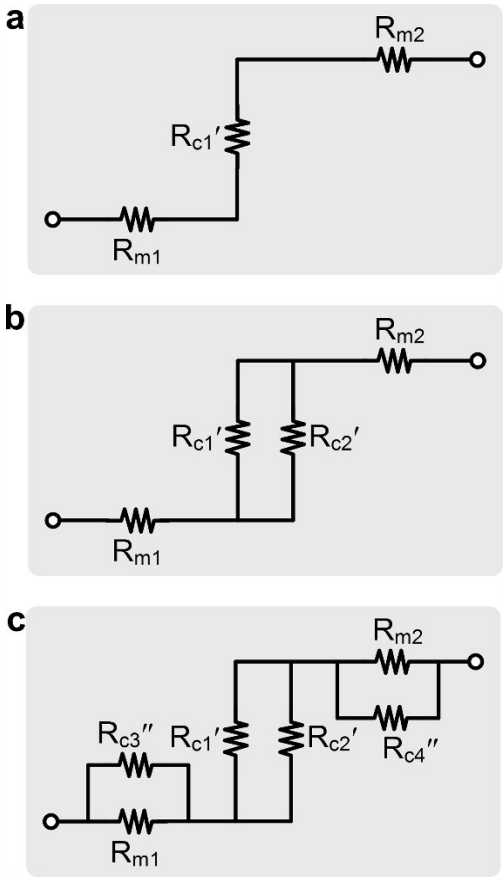

Fig. S5. The simplified equivalent circuit diagrams of the HDM haptic sensor under the states of (**a**) gentle force, (**b**) medium force, and (**c**) heavy force, respectively. Under the gentle force, the two external layers with surface microstructure first make contact. The total resistance (R_t) is simplified as: $R_t = R_{m1} + R_{m2} + R_{c1}'$, where R_{m1} and R_{m2} are the resistance of the upper and bottom conductive microstructure substrates, respectively, R_{c1}' is the contact resistance of the interfaces between the upper and bottom conductive microstructure substrates under gentle force. Under the medium force, the resistance of the device decreases with the increase of the number of contact points due to the larger force. Therefore, the total resistance is calculated as: $R_t = R_{m1} + R_{m2} + R_{c1}'R_{c2}'/(R_{c1}' + R_{c2}')$, where R_{c2}' is the contact resistance of the interfaces between the upper and bottom conductive microstructure substrates under medium force. The further increasing force is detected by the sensing unit, which is based on the contact state between the external and internal conductive layers with surface microstructure. So, the total resistance of the HDM haptic sensor can be expressed as: $R_t = R_{m1}R_{c3}''/(R_{m1} + R_{c3}'') + R_{m2}R_{c4}''/(R_{m2} + R_{c4}'') + R_{c1}'R_{c2}'/(R_{c1}' + R_{c2}')$, where R_{c3}'' is the contact resistance of the interfaces between the bottom and internal conductive microstructure substrate, R_{c4}'' is the contact resistance of the interfaces between the upper and internal conductive microstructure substrate.

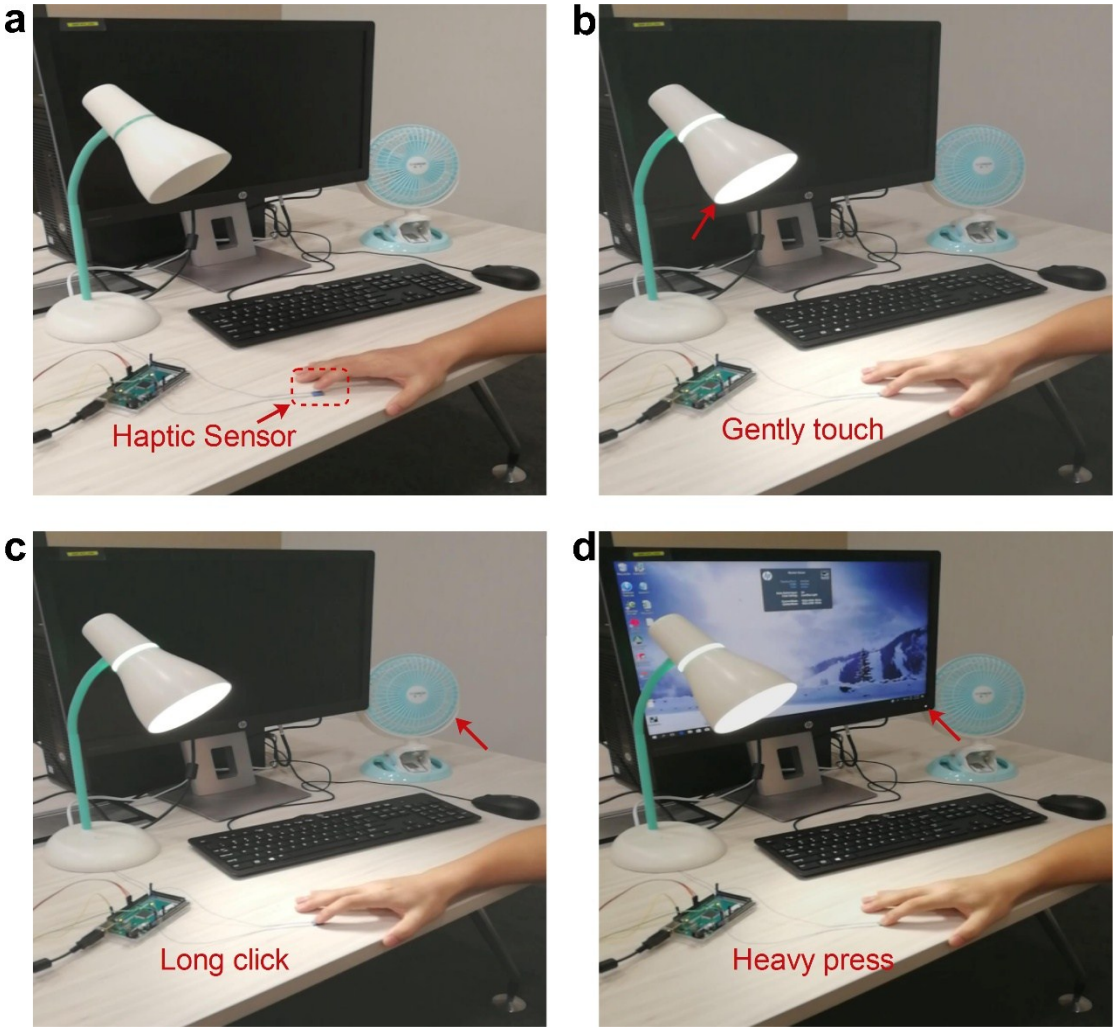

Fig. S6. Diagram of one HDM haptic sensor used to discriminatively control three different electrical appliances. (**a**) Photograph of smart branch console system of multiple electrical appliances based on only one HDM haptic sensor. (**b**) Photograph of the glowing desk lamp through gentle touching on the HDM haptic sensor. (**c**) Photograph of the running electric fan through long clicking on the HDM haptic sensor. (**d**) Photograph of the opening computer screen through heavy pressing on the HDM haptic sensor.

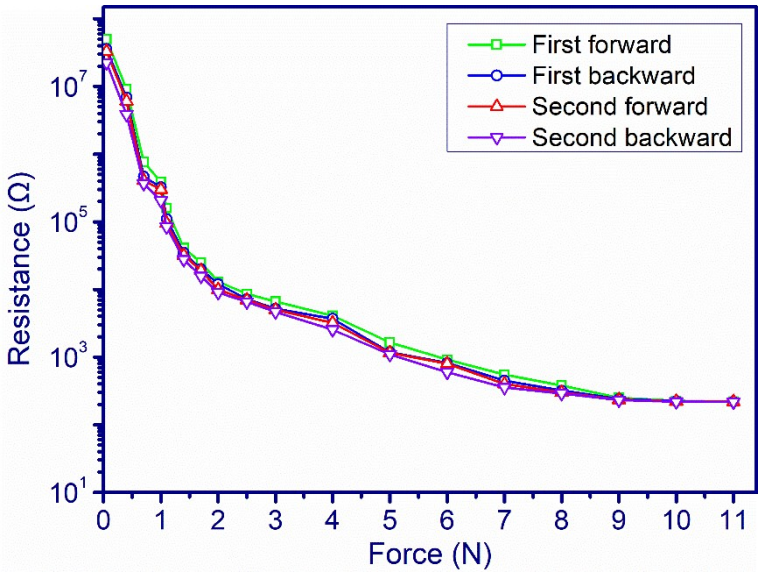

Fig. S7. The consecutive pressure responses of the HMD haptic sensor. The result showed the reproducible pressure response of the HDM haptic sensor.

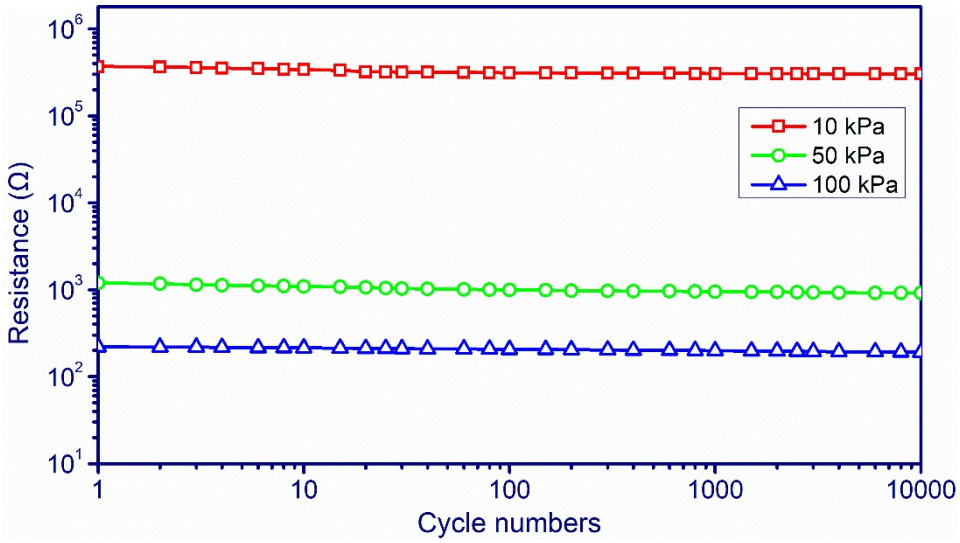

Fig. S8. The value of resistance response of the HDM haptic sensor under the pressure of 10, 50, and 100 kPa during different loading cycles. Notably, after 10,000 pressure loading-unloading cycles, the values of resistance response only reduce 17.7%, 23.5%, and 13.2% corresponding to the pressure of 10, 50, and 100 kPa, respectively.

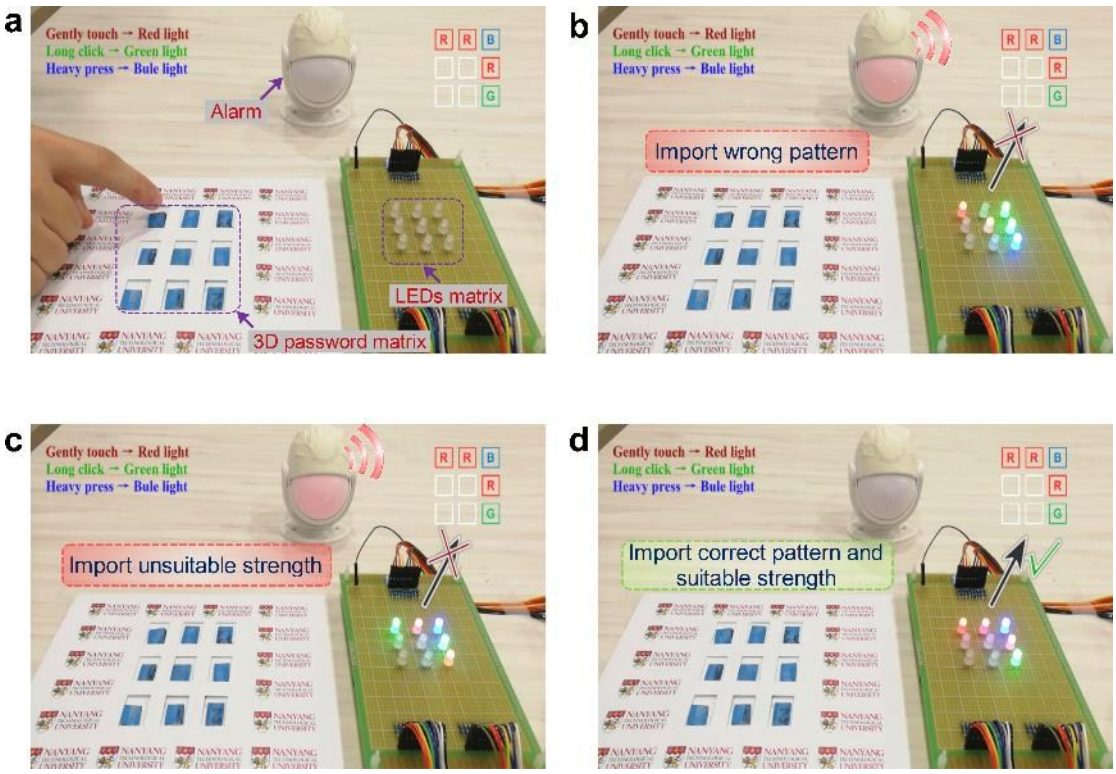

Fig. S9. (**a**) Photograph of the force-enhanced security system based on the three-dimensional (3D) password matrix integrated with the HDM haptic sensors. (**b**, **c**, **d**) Photographs of the color pattern of the light-emitting diodes (LEDs) matrix expressing the input fingertip pressure.

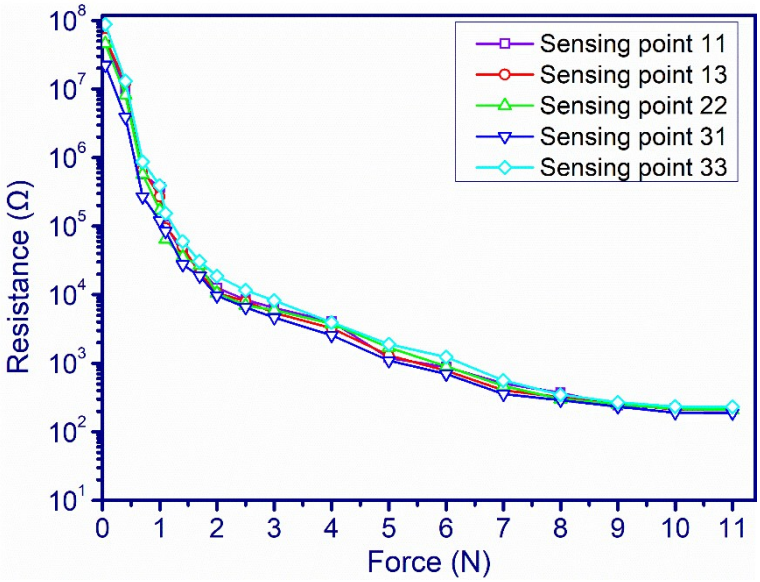

Fig. S10. The typical variations of resistance of multiple HDM haptic sensors under different external force.

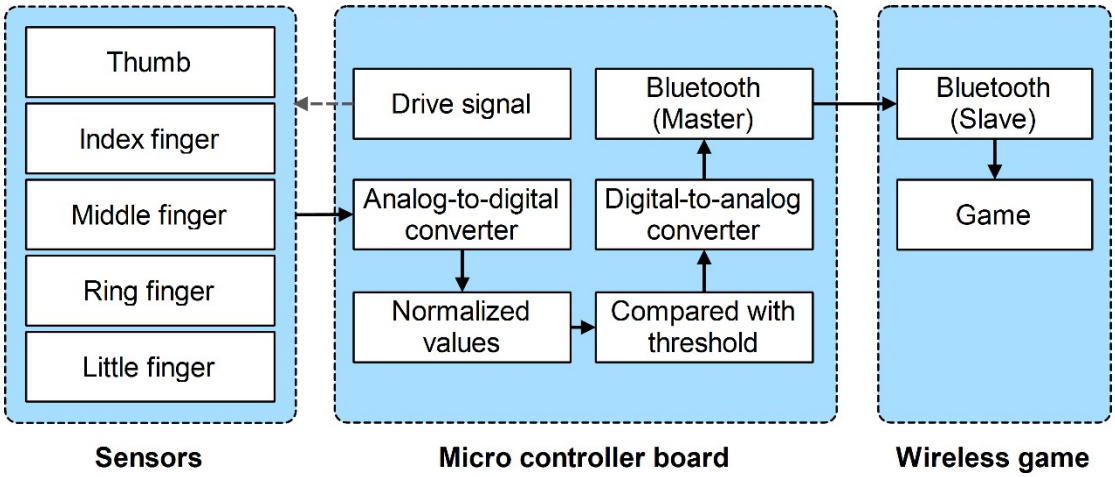

Fig. S11. Flowchart of the wearable wireless interactive entertainment system consisting of five HDM haptic sensors.

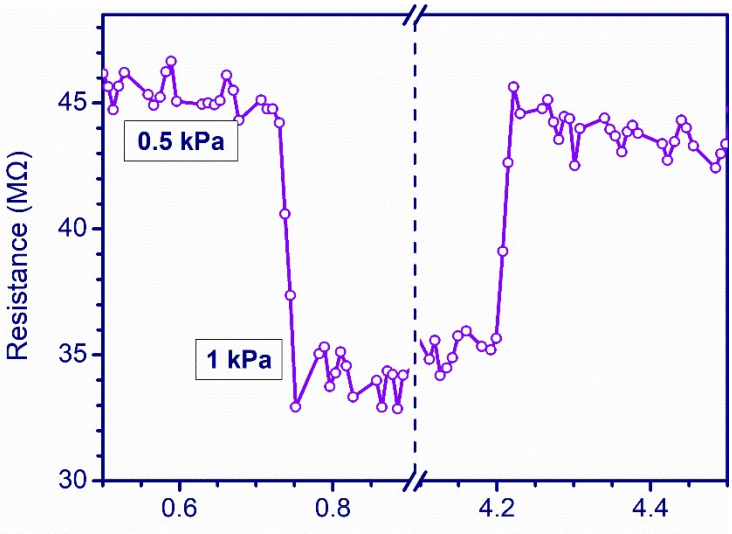

Fig. S12. Drop and rise time of the HDM haptic sensor. The drop time and rise time of the HDM haptic sensor are 21 ms and 22 ms, respectively.

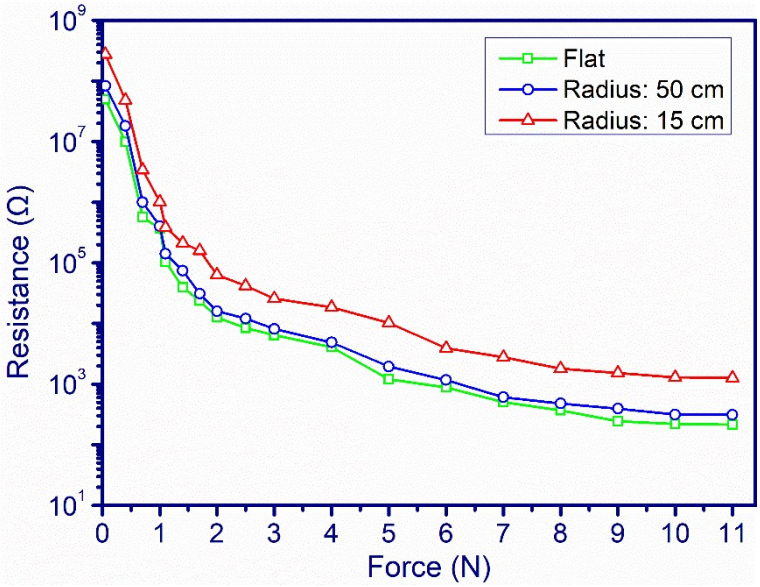

Fig. S13. The resistance of the HDM haptic sensor *versus* external force under different radius of curvature.

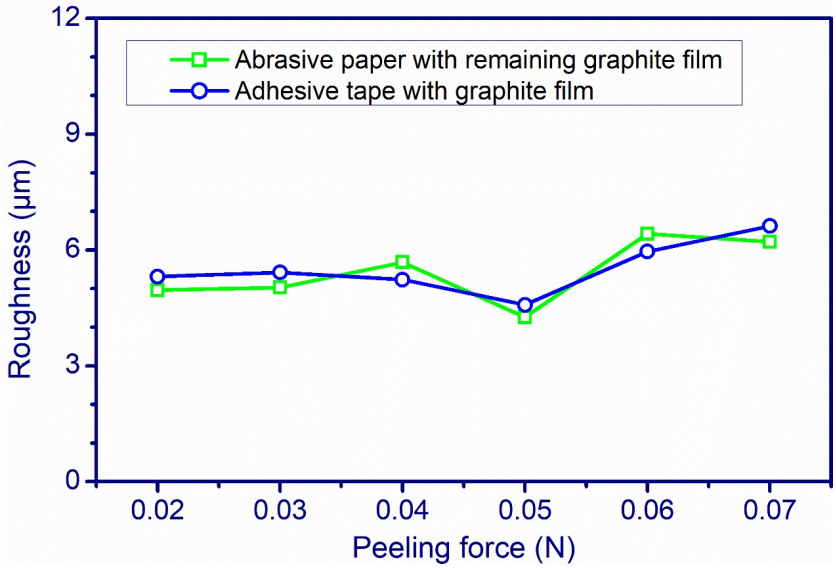

Fig. S14. The relationship between the peeling force and the roughness of the substrates from roughness profiles.